Mechanics of Materials 143 (2020) 103263

Contents lists available at ScienceDirect

Mechanics of Materials

journal homepage: www.elsevier.com/locate/mechmat

Research paper

Thermo-mechanical behavior prediction of shape memory polymer based on the multiplicative decomposition of the deformation gradient

Wei Zhao[a], Liwu Liu[a], Jinsong Leng[b,*], Yanju Liu[a,*]

[a] *Department of Astronautical Science and Mechanics, Harbin Institute of Technology (HIT), P.O. Box 301, No. 92 West Dazhi Street, Harbin 150001, People's Republic of China*

[b] *National Key Laboratory of Science and Technology on Advanced Composites in Special Environments, Harbin Institute of Technology (HIT), P.O. Box 3011, No. 2 YiKuang Street, Harbin 150080, People's Republic of China*

ARTICLE INFO

Keywords:
Shape memory polymer
Constitutive model
Viscoelastic
Phase transition
Thermal-mechanical

ABSTRACT

During the service of shape memory polymer (SMP), the thermal-mechanical cycle is a necessary process. Meanwhile, the influence of the viscoelastic properties of SMP, such as rate-dependent behaviors, can not be ignored during the application. Consequently, a constitutive model based on the multiplicative decomposition of the deformation gradient is proposed in this work, which can clearly describe the viscoelastic behavior and capture the thermal-mechanical cycle process of SMP. By introducing the "phase transition" concept, SMP is assumed as a composite composed of glassy phase and rubbery phase, and the volume fractions of each phase vary with temperature. Furthermore, according to the different mechanical behaviors of the glassy phase and rubbery phase, two different constitutive structures that can describe the strain sensitivity of SMP are developed to represent the mechanical response. The developed model was verified by simulating a series of experiments, including strain sensitivity tests and thermal-mechanical cycle experiments.

1. Introduction

Shape memory polymer (SMP) is a type of material that can recover from a deformation state to its original shape under the appropriate external stimulus. Compared with other smart materials, SMP exhibits many advantages, such as lightweight, high strain recovery, easy processing, low cost and etc. (Zhao et al., 2019; Zhao et al., 2018), which make it has a promising application prospect in fields of aerospace (Liu et al., 2019), medical treatment (Zhao et al., 2017), textile (Castano et al., 2014), microelectronic communication, and etc. For decades, many kinds of SMP are developed to meet different requirements and endowed with a variety of functions. According to different actuation mechanism, SMP can be divided into temperature-driven SMP (Liu et al., 2018), electrical-driven SMP (Leng et al., 2011), magnetic-driven SMP (Meiorin et al., 2018), light-driven SMP (Kuenstler et al., 2019), solution-driven SMP (Urbina et al., 2019) and etc. Moreover, it has become possible to control the glass transition temperature T_g by adjusting the chemical composition and molecular structure with the development of polymer science.

SMP based structures usually involve complex deformation and are in a complicated stress state. Consequently, it is of high importance to predict the deformation history and optimize the recovery performance of SMP, which will contribute to the development of novel SMP and help to understand its complex thermodynamic mechanisms. At present, the constitutive model of SMP can be summarized into three categories, including rheological methods based on viscoelastic theory (Diani et al., 2012; Yin et al., 2019; Mao et al., 2019), microscopic mechanics methods based on "phase transition concept" (Nguyen et al., 2008; Lu et al., 2019) and the modeling methods combining the two methods mentioned above (Qi et al., 2008; Park et al., 2016). The constitutive model based on rheological theory can capture and clearly describe the rate-dependent behavior of SMP, such as relaxation and creep behavior.

Based on the traditional linear viscoelastic three-element model, the phenomenological constitutive equation of four-element thermodynamics was established by Tobushi et al. (2001), where a sliding friction element was introduced to describe the thermomechanical behavior of SMP. Since the time-related parameters were not considered in this model, which greatly limited its forecasting ability. The simulation results related to temperature were not in good agreement with the experimental results. Subsequently, a 3D constitutive model of finite deformation was proposed by Diani et al. (2012) based on the framework of thermodynamic theory and linear viscoelastic model. According to thermodynamic theories, when the temperature is higher

---

* Corresponding authors.
E-mail addresses: lengjs@hit.edu.cn (J. Leng), yj_liu@hit.edu.cn (Y. Liu).

https://doi.org/10.1016/j.mechmat.2019.103263
Received 22 May 2019; Received in revised form 23 November 2019; Accepted 25 November 2019

than the transition temperature, the change of deformation energy is mainly caused by the change of entropy. However, when the temperature is lower than the transition temperature, the variation of deformation energy is mainly caused by the change of cohesive energy (Xie et al., 2014). Besides, the storage and release mechanisms of strain are not taken into account, which greatly limited the use of such models.

However, based on the "phase transition" concept, it is possible to interpret the strain storage and release mechanisms reasonably. Meanwhile, related parameters can be easily obtained by mechanical experiments or simulations. In 2006, a constitutive model considering the microstructure of phase transition (glassy phase and rubbery phase) was developed by Liu et al. (2006) to investigate the strain and stress recovery behavior of SMP. Subsequently, a nonlinear viscoelastic model was established by Chen and Lagoudas (2008) to describe the thermo-mechanical behavior of SMP. Based on the kinematics theory, it was assumed that SMP could realize phase transition through a series of crystal nucleation molding. That was to say, the glassy phase and rubbery phase of SMP could transform each other along with the change of temperature (Lv et al., 2013). However, this type of models is limited to the thermos-elastic theoretical framework due to specific assumptions, and time-dependent properties can not be well explained.

Specifically, if these two types of models combine together, the advantages are complementary. Consequently, a three-dimensional finite deformation constitutive model was developed by Qi et al. to describe the complex multi-axial thermodynamic behavior of SMP, where the "the first-order phase transition" concept was adopted to describe the transformation between glassy phase and rubbery phase (Qi et al., 2008). In this work, it was assumed that SMP was composed of glassy phase and rubbery phase, and the glassy phase could be further divided into the initial glassy phase and frozen glassy phase according to the different heating stages. Subsequently, based on the phenomenological method, a thermodynamic constitutive model was proposed by kim to predict the deformation of shape memory polyurethane, which contained a viscoelastic-induced hard segment and two hyperelastic-induced soft segments (Kim et al., 2010). Two soft segments were corresponding to the frozen phase and the active phase proposed by Liu et al. (2006), respectively. Based on Kim's work, Gu et al. (2015) modified this model by introducing an affine network to describe the stress-strain behavior of the two soft segments and developed a four-element viscoelastic model to simulate the thermal-mechanical behavior of SMP.

In summary, most of the existing models focus on the description of thermal-mechanical behavior, but some limitations still exist in the predication of viscoelastic behavior. Even though the aforementioned modeling methods are important for the development of SMP, some shortcomings cannot be ignored. Under finite deformation, SMP exhibits obvious nonlinear viscoelastic behaviors, including stress relaxation behavior, creep behavior and strain sensitivity, which are equally important to thoroughly explore the material properties of SMP. In existing models, nonlinear viscoelastic behavior is usually regarded as the superposition of rate-independent equilibrium part and viscosity-induced non-equilibrium part. However, it is found that the models that an equilibrium part in parallel with a non-equilibrium part may not be very effective in predicting strain sensitivity of SMP.

Accordingly, a finite strain theory combining the "phase transformation" concept and rheological method is established in this work to predict the thermo-mechanical response and strain sensitivity behavior based on the basic understanding of the molecular structure of SMP. In this model, SMP is regarded as a "composite material" composed of glassy phase and rubbery phase, which will have different volume fractions under different temperatures. Based on the framework of the multiplicative decomposition of the deformation gradient, the thermal-mechanical behavior of the glassy phase is modeled by using two paralleled Maxwell elements and a thermal expansion element. Moreover, the mechanical behavior of the rubbery phase is modeled by using a spring-like hyperelastic element in parallel with a Maxwell element, and the thermal strain was modeled by a thermal expansion element. By introducing an evolutionary equation of volume fractions changing with temperature, the finite strain constitutive model of SMP is developed based on the "phase transformation" assumption. The related parameters of this model are obtained by thermal-mechanical cycle experiments, thermal expansion experiments, dynamic mechanical analyses, rate-dependent tests, and loading/unloading cycle tests. Finally, simulations of the thermal-mechanical cycles and rate-dependent behavior are carried out to validate the developed model.

2. Experimental methods and results

2.1. Material

The SMP material used in this work is the styrene-based thermosetting polymer, which is provided by the National Key Laboratory of Science and Technology on Advanced Composites in Special Environments, Harbin Institute of Technology. The synthetic method can be found in reference Zhang et al. (2011). In the curing process, the styrene solution is poured into a glass panel mold and cured in a vacuum oven following the recommended preparation method.

2.2. Dynamic mechanical analysis

The dynamic thermomechanical analysis (DMA) test was conducted on a DMA Q800 (TA Corporation) machine to explore the thermal-mechanical properties of SMP under different temperatures. The rectangular sample was 2 mm in thickness, 3 mm in width and 20 mm in length. Firstly, the specimen was heated to 20 °C in the DMA machine chamber and stabilized for 15 min to ensure sufficient heat exchange. Subsequently, the tension mode was adopted and a preload of 1mN was implemented on the sample. The sample oscillated at a frequency of 5 Hz while the temperature was heated from 20 °C to 100 °C with a heating rate of 2.5 °C/min. After the sample was heated to 100 °C, it was stabilized for 15 mins and cooled down to 20 °C again at the same rate. This procedure was repeated three times and the data of the last cycle was adopted to illustrate the storage modulus and loss angle tangent value (Tan δ) changing with temperature, as shown in Fig. 1. From the experiment curve, it can be seen that the storage modulus gradually decreases with the increase of temperature. For instance, the storage modulus is about 1800 MPa at 20 °C while it is only 2 MPa at 100 °C, which reduces by about 1000 times. Furthermore, the peak value of the Tan δ curve is identified as the glass transition temperature T_g, which is 67°C.

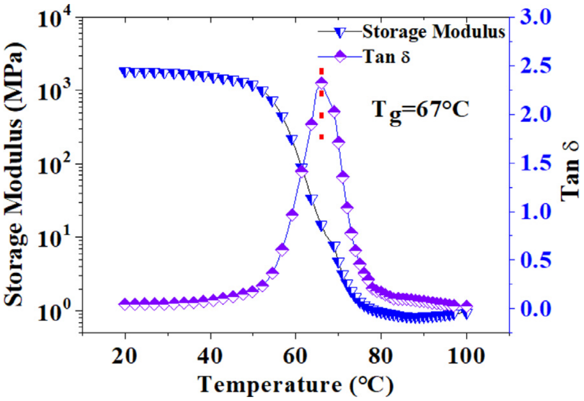

Fig. 1. Results of storage modulus and tan δ from DMA with a heating rate of 2.5 °C/min and a frequency of 5 Hz.

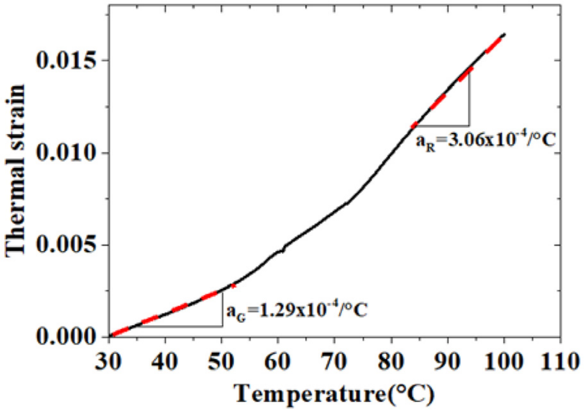

Fig. 2. Thermal expansion experiment to obtain the coefficient of thermal expansion of the shape memory polymer.

2.3. Thermal expansion experiment

As a type of viscoelastic material, the mechanical properties of SMP are highly sensitive to temperature. Moreover, the temperature change is involved throughout the thermal-mechanical cycle of SMP. With the change of temperature, the deformation due to thermal expansion is significant and cannot be neglected. The test of thermal expansion performance of styrene-based SMP was performed on a DMA Q800 (TA Corporation) machine, and the dimension of the rectangular specimen was 2 mm × 3 mm × 20 mm. The ambient temperature was set ranging from 20 °C to 100 °C with a heating rate of 1 °C/min. The specimen was first heated to 20°C and kept for 15 min to ensure sufficient heat exchange, and then a preload of 1 mN was applied. The deformation due to thermal expansion changing with temperature is illustrated in Fig. 2. It can be seen that the rate of thermal deformation shows a sharp turn in the vicinity of T_g. When the temperature is lower than T_g, the thermal deformation rate is slow, and when the temperature is higher than T_g, the thermal deformation rate is fast. The parts marked by the red dash lines at the temperature above and below T_g are used to obtain CTE of the rubbery phase and glassy phase. The CTE below T_g is obtained by using the dash lines of the curve between 30 °C and 53 °C, and the CTE above T_g is obtained by using the dash lines of the curve between 85°C and 100 °C. Here, the corresponding coefficients of thermal expansion for the rubbery phase and the glassy phase are $\alpha_R = 3.06 \times 10^{-4}$/°C and $\alpha_G = 1.29 \times 10^{-4}$/°C, respectively.

2.4. Uniaxial tensile tests

2.4.1. Rate-dependent tests

Generally, rate-dependent behavior is one of the most important properties of viscoelastic material. Due to the difference in molecular microstructure, the polymer exhibits different mechanical responses under different loading rates and shows great dispersion. When the loading rate is high, the stress-strain response is less affected by the microstructure of molecules. Otherwise, the microstructure of molecules will be the dominant factor in the stress-strain response. With the increase of loading rate, the deformation due to viscosity will decrease under the same strain while elastic deformation will increase. Consequently, the sample with a lower loading rate will need a greater load to generate the same deformation comparing with the sample with a higher loading rate.

As a typical viscoelastic material, SMP exhibits obvious rate-dependent behavior under different loading rates. Even at elevated temperature, the strain sensitivity is still evident. The rate-dependent test was performed on a ZWICK-010 universal testing machine with a temperature-controlled cabinet, and the dumbbell-shaped samples were prepared according to the standard of ASTM D638, Type IV (115 mm × 5.8 mm × 2.8 mm). SMP Sample was first heated to 90 °C in a temperature-controlled cabinet and stabilized for 15 min to ensure sufficient heat exchange. Subsequently, the sample was tested with loading rates of 1 mm/min, 500 mm/min and 1000 mm/min, respectively. Experimental results exhibited obvious rate-dependent property as shown in Fig. 3. For instance, mechanical strength was 1.96 MPa, 1.75 MPa and 1.16 MPa with the loading rates being 1 mm/min, 500 mm/min and 1000 mm/min, respectively.

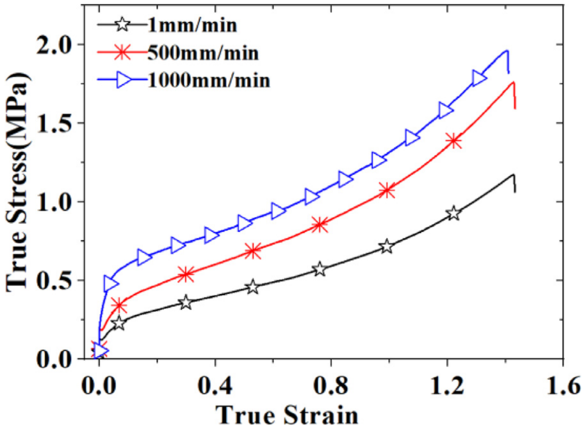

Fig. 3. Rate-dependent tests at 90 °C with loading rates being 1 mm/min, 500 mm/min and 1000 mm/min.

Furthermore, under the same condition and standard, the samples were tested with loading rates of 1 mm/min and 100 mm/min at the temperature of 30 °C, 40 °C and 50 °C as shown in Fig. 4. The rate-dependent behavior is extremely obvious, and the load at a loading rate of 100 mm/min is much higher than that of 1 mm/min under the same strain. Furthermore, the difference between them becomes increasingly obvious with the increase of temperature, which indicates that the strain sensitivity is enhanced in the vicinity of T_g.

2.4.2. Loading/unloading cycle tests

Guided by similar developments in the field of rate-dependent model for polymer (Qi et al., 2005), loading-unloading experiments with a wide range of loading rates were conducted in this work. The samples (ASTM D638, Type IV, 115 mm × 5.8 mm × 2.8 mm) were first placed in a temperature-controlled cabinet and heated to 35 °C. After stabilizing for 15 min, the samples were stretched by 3.07×10^{-2} true strain and unloaded it with the same loading rate until the stress reduced to zero. The loading rates of five group tests were 1 mm/min, 5 mm/min, 10 mm/min, 20 mm/min and 50 mm/min, as shown in Fig. 5. From the experimental results, it can be obtained that under the same strain, the higher the loading rate is, the greater the load is. The maximum loads are 23.01 MPa, 22.06 MPa, 16.16 MPa, 12.97 MPa and 9.65 MPa when the strain is 3.07×10^{-2}. Furthermore, it is worth mentioning that when the stress reduces to zero in the unloading process, the strain is not fully recovered, which is caused by viscosity deformation.

2.5. Thermo-mechanical cycle experiment

According to the theory of thermodynamics, there are two types of deformation mechanism of SMP: conformational entropy motion and the non-conformational motion. When SMP is in the rubbery state, the entropy will decrease with the increase of deformation. However, when SMP is in the glassy state, the conformational position of polymer chains will be frozen. Moreover, entropy change induced by deformation will be stored in the form of free energy, and reheating SMP to a high temperature, the free energy will be released again. The thermo-mechanical cycle experiment perfectly reproduces the storage and release process of free energy.

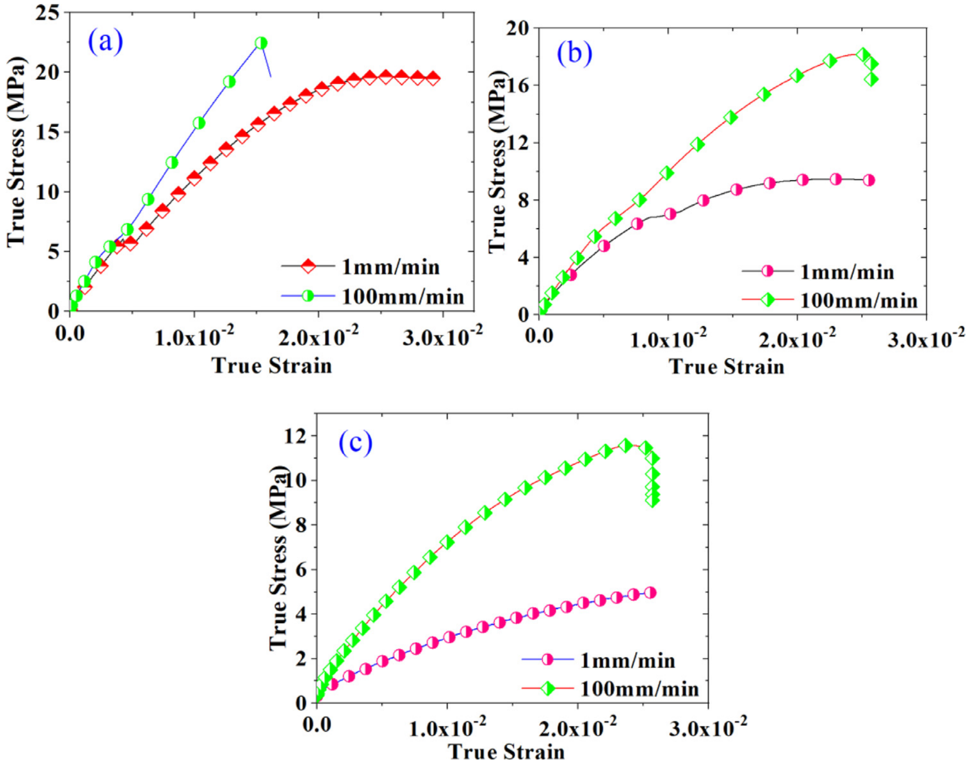

Fig. 4. Rate-dependent tests at (a) 30 °C (b) 40 °C and (c) 50 °C with strain rates being 1 mm/min, 100 mm/min.

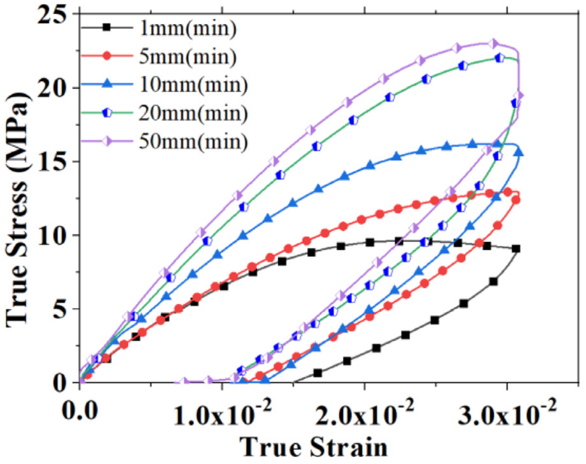

Fig. 5. Rate-dependent tests at 35 °C with loading rates being 1 mm/min, 5 mm/min, 10 mm/min, 20 mm/min and 50 mm/min.

In this work, the thermal-mechanical cycle experiment was performed on a ZWICK-010 universal testing machine with a sample dimension of 115 mm × 5.8 mm × 2.8 mm (ASTM D638, Type IV). The whole process of thermal-mechanical cycle was set as: Step 1-Heat the sample to 90 °C with a heating rate of 2 °C/min and stabilize for 15 min; Step 2-Apply 15% strain on sample with a loading rate of 2 mm/min; Step 3-Cool down the temperature to 20 °C with a cooling rate of 2 °C/min while restrain the deformation; Step 4-Unload the stress until it reduces to zero; Step 5-Reheat the sample to 90 °C with a heating rate of 2 °C/min. From the experimental results (Fig. 6), it can be seen that the initial stress is about 0.1 MPa (step 2), and after the cooling process (step 3), the stress increases to 1.8 MPa as shown in Fig. 6(a) and (b). The thermal contraction of SMP under the confined boundary condition results in the increase of stress. Besides, the shape recovery ratio of SMP is close to 100% as shown in Fig. 6(c).

3. Constitutive model

3.1. Overall model description

The schematic of the proposed constitutive model is presented in Fig. 7. Here, SMP is assumed as a composite material, which is composed of the rubbery phase and glassy phase as shown in Fig. 7(a). Moreover, the volume fractions of the two phases will change in response to temperature. The whole strain (ε) consists of thermal strain (ε_T), mechanical strain (ε_M) and shape memory strain (ε_{sm}) as shown in Fig. 7(b), where the thermal expansion elements are arranged in series with mechanical elements. Two groups of Maxwell elements, i.e. an elastic element in series with a viscous element, are introduced to simulate the mechanical behavior of the glassy phase while a hyperelastic network in paralleled with a Maxwell network are used to describe the mechanical behavior of rubbery phase. The network representing the glassy phase and the parallel network representing the rubbery phase are combined together to characterize the mechanical behavior of SMP. Moreover, another element representing shape memory strain is introduced into the model of the glassy phase. During the cooling process, the mechanical deformation at the rubbery state will be transformed to shape memory strain and stored in this component. For simplicity, the multiplicative split of the deformation gradient into thermal and mechanical components is introduced to separate thermal deformation and mechanical deformation:

$$\mathbf{F} = \mathbf{F}_M\mathbf{F}_T \tag{1}$$

where $\mathbf{F}$ is the total deformation gradient, the notation $\mathbf{F}_\mathrm{M}$ is mechanical deformation gradient and $\mathbf{F}_\mathrm{T}$ is thermal deformation gradient.

3.2. Constitutive equations for volumetric deformation

The volumetric deformation can be divided into mechanical component and thermal deformation component, which can be expressed as: $\Theta = \Theta_M\Theta_\mathrm{T}$. Without loss of generality, it is assumed that the thermal expansion deformation of SMP is isotropic and independent of the

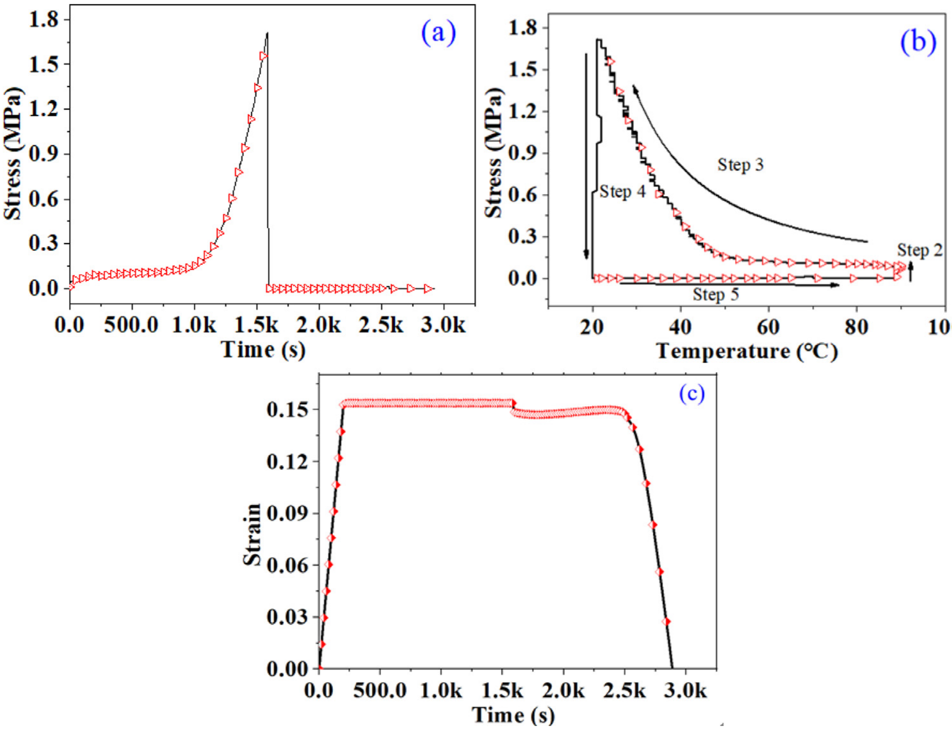

Fig. 6. Thermo-mechanical cycle experiments: (a) stress history (b) stress history changes with temperature (c) strain history.

mechanical properties, which can be expressed as:

$$\mathbf{F}_{\mathrm{T}} = \Theta_{\mathrm{T}}{}^{1/3}\mathbf{I} \tag{2}$$

where $\mathbf{I}$ is the second-order identity tensor and $\Theta_T = \det(\mathbf{F}_T)$ is volume deformation caused by thermal expansion, which can be obtained by $\Theta_T = \frac{V(T)}{V_0}$.

The CTE is different for the glassy phase and rubbery phase, as shown in Fig. 2. When the temperature is below T_g, SMP is in the glassy state, and CTE is $\alpha_G = 1.29 \times 10^{-4}/$ °C. However, when the temperature is above T_g, SMP is in the rubbery state, and CTE is $\alpha_R = 3.06 \times 10^{-4}/$ °C. The volume ratio Θ_T in the different states can be expressed as follows. For the rubbery phase of SMP, the thermal expansion deformation Θ_{T_R} can be expressed as:

$$\Theta_{T_R} = \frac{V(T)}{V_0} = [1 + \alpha_R(T - T_0)]^3 \tag{3}$$

where T_0 is reference temperature, and V_0 represents reference volume at T_0. Expand it according to Taylor's equation and take the first order:

$$\Theta_{T_R} = 1 + 3\alpha_R(T - T_0) \tag{4}$$

For the glassy phase of SMP, the thermal expansion deformation Θ_{T_G} is of the form:

$$\Theta_{T_G} = \frac{V(T)}{V_0} = [1 + \alpha_G(T - T_0)]^3 \tag{5}$$

Expand it according to Taylor's equation and take the first order:

$$\Theta_{T_G} = 1 + 3\alpha_G(T - T_0) \tag{6}$$

3.3. Evolution rule for volume fractions

According to the "phase transition" assumption, the volume fractions of the rubbery phase and glassy phase change with temperature. In order to obtain the evolution law of volume fraction, the experiment data in thermal-mechanical cycle tests are used to fit the model parameters. The volume fraction of the glassy phase Φ_G can be captured by Eq. (7):

$$\Phi_G = \alpha \cdot exp\left(-\frac{T - T_{r_1}}{\beta}\right) \tag{7}$$

where T_{r_1} represents reference temperature, α and β are fitting parameters. Here, the volume fractions of the glassy phase and rubbery phase should satisfy:

$$\Phi_R + \Phi_G = 1 \tag{8}$$

3.4. Structural relaxation of the rubbery phase

Structural relaxation time is a physical quantity to describe the micro-movement of a molecular network, which is related to the molecular structure, viscosity, modulus and temperature. During the glass transition process, the molecular chains tend to move significantly and reach a balance, in response to the change of ambient temperature (Lendlein and Kelch, 2002). To obtain the best fitting effect and facilitate to adjust the model parameters, the Adam-Gibbs model (Nguyen et al., 2008) is adopted to describe the evolution law of the structural relaxation time of SMP. Meanwhile, the Williams-Landel-Ferry (WLF) equation (Williams et al., 1955) was employed to derive the parameters of SMP in the rubbery phase. The structural relaxation time τ_R of the rubbery phase can be expressed as:

$$\tau_R = \tau_{Rr} exp\left(-\frac{c_1}{loge}\left(\frac{c_2(T - T_v) + T(T - T_{r_2})}{T(c_2 + T_v - T_{r_2})}\right)\right) \tag{9}$$

where τ_{Rr} is the structural relaxation time measured at the reference temperature T_{r_2}. The material parameters c_1,c_2 and T_{r_2} can be obtained by conventional thermal-mechanical test. Specific discussions about the fitting method of material parameters are presented in Appendix A.

3.5. Deformation and stress of the rubbery phase

When the temperature is much higher than T_g, SMP is entirely composed of the rubbery phase. Consequently, the stress-strain responses are determined by the constitutive relation of the rubbery phase represented by networks C and D, as shown in Fig. 8. In this case,

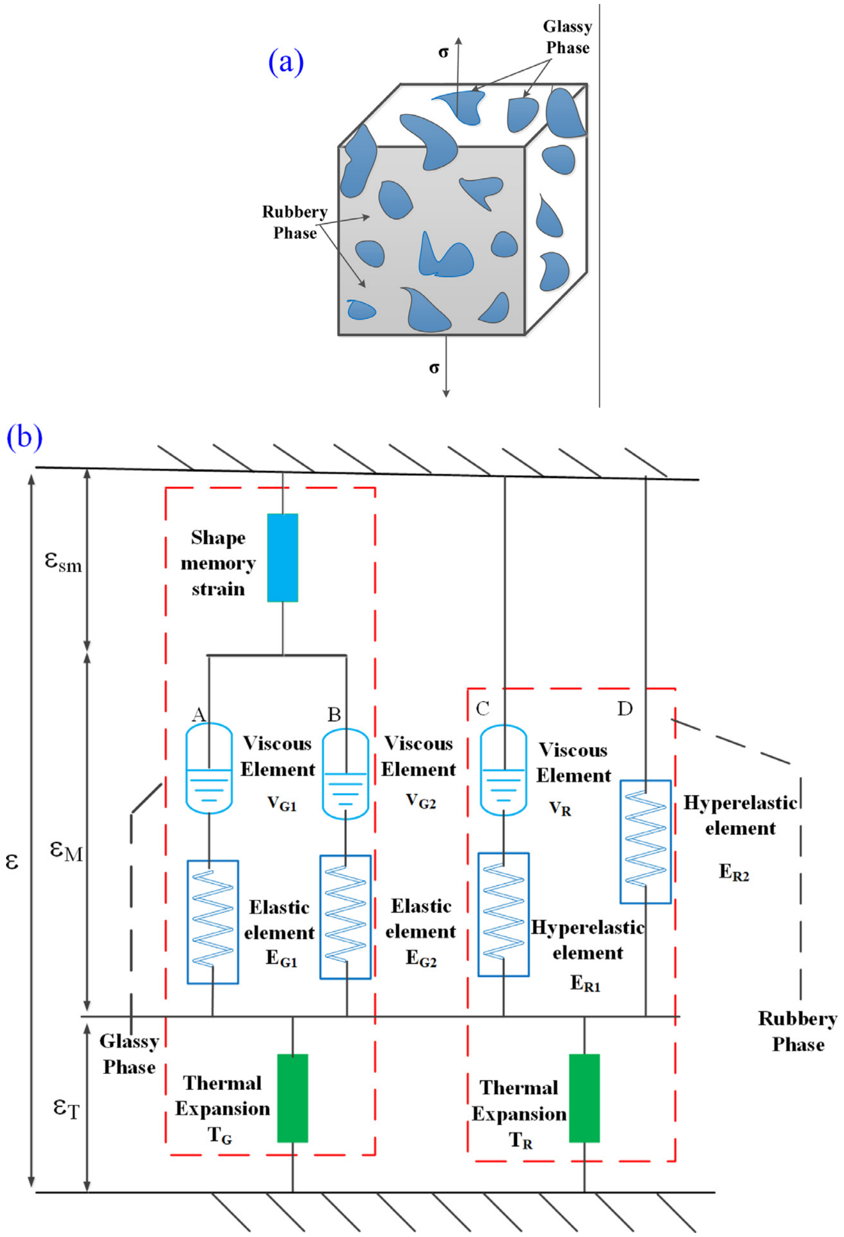

Fig. 7. Schematics of the proposed constitutive model (a) SMP is assumed as a composite comprised of a glassy phase and of a rubbery phase (b) overall framework of the constitutive model.

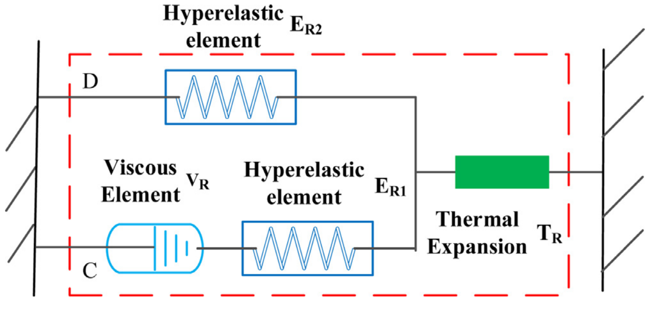

Fig. 8. Schematic of the constitutive relation of the rubbery phase.

the total deformation gradient **F** can be multiplicatively decomposed into the mechanical deformation part $\mathbf{F}_{\mathrm{R}}^{\mathrm{M}}$ and thermal deformation part $\mathbf{F}_{\mathrm{R}}^{\mathrm{T}}$. Further, the mechanical deformation part can be split into elastic deformation part $\mathbf{F}_{R}^{e}$ and viscous deformation part $\mathbf{F}_{R}^{\upsilon}$:

$$\mathbf{F} = \mathbf{F}_{\mathrm{R}}^{\mathrm{M}}\mathbf{F}_{\mathrm{R}}^{\mathrm{T}},\ \mathbf{F}_{\mathrm{R1}}^{\mathrm{M}} = \mathbf{F}_{\mathrm{R}_1}^{\mathrm{e}},\ \mathbf{F}_{\mathrm{R}_1}^{\upsilon} = \mathbf{F}_{\mathrm{R}_2}^{\mathrm{e}} \tag{10}$$

where $\mathbf{F}_{\mathrm{R}_1}^{\upsilon}$ is the relaxed configuration after removing the elastic configuration $\mathbf{F}_{\mathrm{R}_1}^{\mathrm{e}}$(network C), the notation $\mathbf{F}_{\mathrm{R}_2}^{\mathrm{e}}$ is the deformation gradient of network D and $\mathbf{F}_{\mathrm{R}}^{\mathrm{T}}$ is the thermal deformation gradient.

Moreover, the rate of deformation tensors of total deformation $\dot{\mathbf{F}}_{R}^{M}$, elastic part $\dot{\mathbf{F}}_{R}^{e}$ and viscous part $\dot{\mathbf{F}}_{R}^{\upsilon}$ are introduced as follows.

$$\dot{\mathbf{F}}_{R}^{M} = \mathbf{L}_{R}^{M}\mathbf{F}_{R}^{M},\ \dot{\mathbf{F}}_{R}^{e} = \mathbf{L}_{R}^{e}\mathbf{F}_{R}^{e},\ \dot{\mathbf{F}}_{R}^{\upsilon} = \mathbf{L}_{R}^{\upsilon}\mathbf{F}_{R}^{\upsilon} \tag{11}$$

The stress caused by viscoelastic deformation can be obtained by the following equation:

$$\mathbf{L}_{R}^{M} = \mathbf{L}_{R}^{e} + \mathbf{F}_{R}^{e}\mathbf{L}_{R}^{\upsilon}\mathbf{F}_{R}^{e\,-1} \tag{12}$$

where $\mathbf{L}_{\mathrm{R}}^{\upsilon}$ is the viscous spatial velocity gradient. Without loss of generality, the effect caused by viscous spin is neglected during the deformation process. Therefore, the viscous stretch rate tensor can be expressed as:

$$\mathbf{D}_{\mathrm{R}}^{\upsilon} = \mathbf{L}_{\mathrm{R}}^{\upsilon} = \mathbf{L}_{\mathrm{R}}^{\upsilon\,\mathrm{T}},\ \mathbf{L}_{\mathrm{R}}^{\upsilon} = \dot{\mathbf{F}}_{\mathrm{R}}^{\upsilon}\mathbf{F}_{\mathrm{R}}^{\upsilon\,-1} \tag{13}$$

where $\mathbf{D}_{\mathrm{R}}^{\upsilon}$ represents viscous stretch rate tensor, the notation $\mathbf{L}_{\mathrm{R}}^{\upsilon}$ is viscous spatial velocity gradient and notation $\mathbf{F}_{\mathrm{R}}^{\upsilon}$ is viscous deformation gradient tensor. The elastic deformation tensor $\mathbf{D}_{\mathrm{R}}^{e}$ can be expressed as:

$$\mathbf{D}_{\mathrm{R}}^{e} = \frac{1}{2}\mathbf{F}_{k}^{e\,-T}\dot{\mathbf{C}}_{k}^{e}\mathbf{F}_{k}^{e\,-1} \tag{14}$$

with the relation of $\mathbf{C} = \mathbf{F}^{\mathrm{T}}\mathbf{F}$.

3.5.1. *Mooney-Rivlin elasticity of rubbery phase*

As shown in Fig. 8, the rubbery phase network is composed of two hyperelastic elements and a viscous element. Mooney-Rivlin model is adopted to describe the mechanical behavior of the hyperelastic network, which exhibits good applicability in the prediction of moderate deformation conditions. The strain energy density function for the Mooney-Rivlin model is given by:

$$W = c_3(\bar{\mathbf{I}}_1 - 3) + c_4(\bar{\mathbf{I}}_2 - 3) \tag{15}$$

where c_3 and c_4 are the material parameters related to distortion response which can be obtained from the tensile experiment. Besides, notation $\bar{\mathbf{I}}_1$ and $\bar{\mathbf{I}}_2$ are the first and second invariant of $\overline{\mathbf{B}} = (\det\mathbf{B})^{-\frac{1}{3}}\mathbf{B}$:

$$\bar{\mathbf{I}}_1 = J^{-\frac{2}{3}}\mathbf{I}_1,\ \mathbf{I}_1 = \mathrm{trace}(\mathbf{B}) = \lambda_1^2 + \lambda_2^2 + \lambda_3^2 \tag{16a}$$

$$\bar{\mathbf{I}}_2 = J^{-\frac{4}{3}}\mathbf{I}_2,\ \mathbf{I}_2 = \mathrm{trace}(\mathbf{B}\cdot\mathbf{B}) = \lambda_1^2\lambda_2^2 + \lambda_2^2\lambda_3^2 + \lambda_3^2\lambda_1^2 \tag{16b}$$

$$J = \det(\mathbf{F}) = \lambda_1\lambda_2\lambda_3 \tag{16e}$$

where λ_i represents stretch ratio in the principal planar directions, and $\mathbf{F}$ is the deformation gradient. Cauchy stress of the two Mooney-Rivlin models can be given by:

$$\begin{aligned}\sigma_{R_1} &= \frac{2}{J}\left[\frac{1}{J^{\frac{2}{3}}}\left(\frac{\partial W_1}{\partial \bar{\mathbf{I}}_1^{\mathrm{R1}}} + \bar{\mathbf{I}}_2\frac{\partial W_1}{\partial \bar{\mathbf{I}}_2^{\mathrm{R1}}}\right)\mathbf{B}_{\mathrm{R}_1} - \frac{1}{J^{\frac{4}{3}}}\frac{\partial W_1}{\partial \bar{\mathbf{I}}_2^{\mathrm{R1}}}\mathbf{B}_{\mathrm{R}_1}\cdot\mathbf{B}_{\mathrm{R}_1}\right] \\ &\quad + \left[\frac{\partial W_1}{\partial J} - \frac{2}{3J}\left(\bar{\mathbf{I}}_1^{\mathrm{R}_1}\frac{\partial W_1}{\partial \bar{\mathbf{I}}_1^{\mathrm{R1}}} + 2\bar{\mathbf{I}}_2\frac{\partial W_1}{\partial \bar{\mathbf{I}}_2^{\mathrm{R1}}}\right)\right]\mathbf{I}\end{aligned} \tag{17-a}$$

$$\begin{aligned}\sigma_{R_2} &= \frac{2}{J}\left[\frac{1}{J^{\frac{2}{3}}}\left(\frac{\partial W_2}{\partial \bar{\mathbf{I}}_1^{\mathrm{R2}}} + \bar{\mathbf{I}}_2\frac{\partial W_2}{\partial \bar{\mathbf{I}}_2^{\mathrm{R2}}}\right)\mathbf{B}_{\mathrm{R}_2} - \frac{1}{J^{\frac{4}{3}}}\frac{\partial W_2}{\partial \bar{\mathbf{I}}_2^{\mathrm{R2}}}\mathbf{B}_{\mathrm{R}_2}\cdot\mathbf{B}_{\mathrm{R}_2}\right] \\ &\quad + \left[\frac{\partial W_2}{\partial J} - \frac{2}{3J}\left(\bar{\mathbf{I}}_1^{\mathrm{R}_2}\frac{\partial W_1}{\partial \bar{\mathbf{I}}_1^{\mathrm{R2}}} + 2\bar{\mathbf{I}}_2\frac{\partial W_2}{\partial \bar{\mathbf{I}}_2^{\mathrm{R2}}}\right)\right]\mathbf{I}\end{aligned} \tag{17-b}$$

with $\frac{\partial W_1}{\partial \bar{\mathbf{I}}_1} = c_3^{\mathrm{R}_1}$, $\frac{\partial W_1}{\partial \bar{\mathbf{I}}_2} = c_4^{\mathrm{R}_1}$, $\frac{\partial W_2}{\partial \bar{\mathbf{I}}_1} = c_3^{\mathrm{R}_2}$, $\frac{\partial W_2}{\partial \bar{\mathbf{I}}_2} = c_4^{\mathrm{R}_2}$, $\mathbf{B}_{\mathrm{R}_1}^{-1} = \mathbf{B}_{\mathrm{R}_1}\cdot\mathbf{B}_{\mathrm{R}_1} - \mathbf{I}_1^{\mathrm{R}_1}\mathbf{B}_{\mathrm{R}_1} + \mathbf{I}_2^{\mathrm{R}_1}\mathbf{I}$ and $\mathbf{B}_{\mathrm{R}_2}^{-1} = \mathbf{B}_{\mathrm{R}_2}\cdot\mathbf{B}_{\mathrm{R}_2} - \mathbf{I}_2^{\mathrm{R}_2}\mathbf{B}_{\mathrm{R}_2} + \mathbf{I}_2^{\mathrm{R}_2}\mathbf{I}$

3.5.2. *Viscous flow rule of the rubbery phase*

From the rate-dependent test results, as shown in Fig. 3, it can be seen that stress shows great strain sensitivity even at high temperatures. Consequently, it can be concluded that the viscoelasticity response cannot be neglected. A governing equation of viscous flow is introduced to describe its viscoelastic behavior. For the viscous flow of the rubbery phase, it is assumed that the deformation process conforms to the change law of nonlinear Newtonian fluid. The viscous strain rate can be expressed as (Holzapfel et al., 1999):

$$\dot{\gamma}_v = -\frac{\mathrm{s}}{\eta_R} \tag{18}$$

where $\dot{\gamma}_v$ is viscous strain rate of the rubbery phase, notation η_R represents the viscosity parameter of SMP in rubbery state, and s represents the equivalent stress of non-equilibrium state (network C), which can be obtained by the equations $= [\frac{1}{2}\sigma_R\colon \sigma_R]^{\frac{1}{2}} = \|\bar{\sigma}_R\|/\sqrt{2}$. Since the viscosity coefficient varies greatly with temperature, the time-temperature shift factor is introduced into the model to describe the viscosity changing with temperature based on Eyring's work (Westbrook et al., 2011). The extended viscous flowing control equation can be expressed as:

$$\dot{\gamma}_v = \frac{\mathrm{s}_y}{2\eta_{sr}}exp\left[-\frac{c_1}{loge}\left(\frac{T - T_r}{c_2 + T - T_r}\right)\right]sinh\left(\frac{Q_s}{T}\cdot\frac{s}{s_y}\right) \tag{19}$$

where η_{sr} is the viscosity coefficient at the reference temperature T_{r}, s_y represents the yield stress and Q_s is activation energy under the stress-free state. For SMP in the rubbery state, the molecular chain is near equilibrium and satisfies s → 0. Set$Q = exp[-\frac{c_1}{loge}(\frac{T-T_g}{c_2+T-T_g})]$, the equation can be further simplified as:

$$\dot{\gamma}_\upsilon = \frac{1}{2\eta_R}Q||\sigma^{neq}|| \tag{20}$$

Since the viscosity coefficient equation is a function of temperature, the parameter values in the rubbery state at any temperature can be obtained by fitting the stress-strain curve. Based on the Newton fluid assumption, the viscous flow direction is identical to Mandel stress, which can be considered as the driving stress of viscous deformation:

$$\mathbf{M}_{\mathrm{R}} = \eta_{\mathrm{R}}\mathbf{D}_{\mathrm{R}}^{\upsilon} \tag{21}$$

where $\mathbf{M}_{\mathrm{R}}$: =dev($\mathbf{C}_e\mathbf{S}$) is Mandel stress (Chen et al., 2014), $\mathbf{C}_e = \mathbf{F}_e^T\mathbf{F}_e$ is the right Cauchy-Green deformation tensor, and $\mathbf{S} = J_{\mathrm{R}}^{\mathrm{e}}\mathbf{F}_e^{-1}\bar{\sigma}_R\mathbf{F}_e^{-T}$ is the second Piola-Kirchoff stress tensor. The control equation of viscous deformation can be further expressed as:

$$\dot{\mathbf{F}}_R^{\upsilon} = -\frac{1}{\eta_{\mathrm{R}}}\mathbf{M}_{\mathrm{R}}\mathbf{F}_{\mathrm{R}}^{\upsilon} \tag{22}$$

3.6. *Deformation and stress of the glassy phase*

In this work, the concept of the modified equilibrium path is introduced to describe the viscoelastic behavior of the glassy phase. Generally, the Zener type (Qi et al., 2005) model (a Maxwell model in parallel with a spring) is widely used because it can effectively describe the nonlinear viscoelastic behavior of the polymer. According to the Zener type model, the stress-strain curve of the loading-unloading experiment can be divided into two parts: the equilibrium path part and the overstress contribution part. The mechanical response represented by the equilibrium path is the rate-independent part and corresponds to the average value of stress-strain. Taking the mid-path of the loading-unloading curve, the two parts can be determined (Bergström et al., 1998) after a series of calculations. Generally, the mechanical contribution of the rate-independent part can be described by a spring-like element while the rate-dependent part is described by a Maxwell element.

The average stress-strain curves corresponding to the equilibrium path can be calculated by the loading-unloading experiment as shown in Fig. 5. However, the experimental results indicated that the mechanical response of the glassy phase was not consistent with the characteristic of the Zener type model. The identified equilibrium paths were closely related to loading rates, and its change trend conformed to a power-law relation. Consequently, it can be concluded that the mechanical behavior of styrene-based SMP does not conform to the mechanical response described by the "equilibrium path" of the Zener type model.

Due to the apparent rate-dependent behavior of the contribution represented by the so-called "equilibrium path" part, a modified model is introduced in this work, where the single spring element in the Zener type model is substituted by another Maxwell element. As shown in Fig. 9, two paralleled Maxwell elements are employed to describe the nonlinear viscoelastic behavior of SMP in the glassy state. The contribution of the elastic part is illustrated by network A while the viscosity-induced hysteresis response is represented by network B. Besides, the component of shape memory strain is added in this model, which represents the transformed strain of rubbery phase during the cooling process.

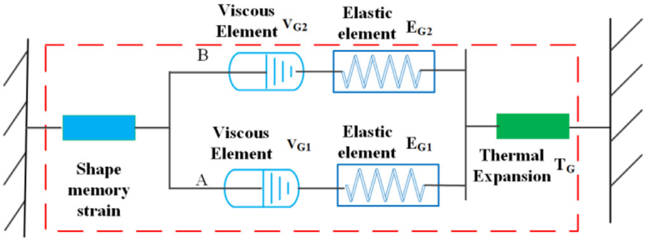

Fig. 9. Schematic of the constitutive relation of the glassy phase.

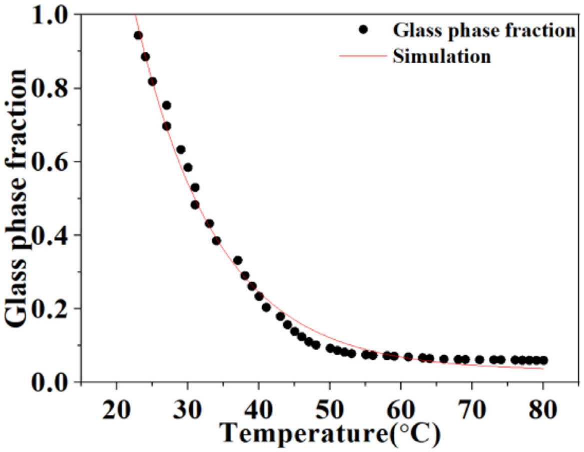

Fig. 10. Identification of the model parameters for phase transition process.

The total deformation gradient can be multiplicatively decomposed into the mechanical deformation gradient $\mathbf{F}_{\mathrm{G}}^{\mathrm{M}}$and thermal deformation gradient$\mathbf{F}_{\mathrm{G}}^{\mathrm{T}}$. Furthermore, the coupling deformation of the elastic part and the viscoelastic part is considered as the main cause of the mechanical deformation of SMP. According to Taylor assumption, the mechanical deformation gradient $\mathbf{F}$ can be further decomposed into an elastic part $\mathbf{F}_{\mathrm{G}}^{\mathrm{e}}$ and a viscous part $\mathbf{F}_{\mathrm{G}}^{\upsilon}$:

$$\mathbf{F} = \mathbf{F}_{\mathrm{G}}^{\mathrm{M}}\mathbf{F}_{\mathrm{G}}^{\mathrm{T}},\ \mathbf{F}_{\mathrm{G}}^{\mathrm{M}} = \mathbf{F}_{\mathrm{G}_1}^{\mathrm{e}}\mathbf{F}_{\mathrm{G}_1}^{\upsilon} = \mathbf{F}_{G_2}^{\mathrm{e}}\mathbf{F}_{G_2}^{\upsilon} \tag{23}$$

where $\mathbf{F}_{\mathrm{G}_1}^{\mathrm{e}}$ and $\mathbf{F}_{G_2}^{e}$ are the elastic deformation part of network A and B while $\mathbf{F}_{\mathrm{G}1}^{\upsilon}$ and $\mathbf{F}_{G_2}^{\upsilon}$ are the viscous deformation part of network A and B, respectively.

3.6.1. Hencky's elasticity of glassy phase

Hencky's strain-energy function (Hencky, 1928) is widely used to predict the moderate deformation of metal and elastomers, which is in good agreement with experimental results (Anand, 1979). In this work, the mechanical behavior of the elastic element of the glassy phase is described by the Hencky model. The strain ε in classical Hooke's law is substituted by natural logarithm $ln\lambda$, which λ represents a stretch ratio. The nonlinear strain energy equation describing material elasticity can be expressed as:

$$W_{G_1} = \mu_{G_1}\prod_{2}^{G_1} + \frac{k_{G_1}}{2}\left(\prod_{1}^{G_1}\right)^2 \tag{24a}$$

$$W_{G_2} = \mu_{G_2}\prod_{2}^{G_2} + \frac{k_{G_2}}{2}\left(\prod_{1}^{G_2}\right)^2 \tag{24b}$$

where μ_G and $\frac{k}{2}$ are Lame elastic constant, and $\prod_i = (\ln\lambda_1)^i + (\ln\lambda_2)^i + (\ln\lambda_3)^i$, $i = 1, 2, 3$ is Hencky variable. The corresponding finite stress-strain relation can be expressed as:

$$\boldsymbol{\tau}_{G_1} = J\boldsymbol{\sigma}_{G_1} = \frac{\partial W}{\partial \prod_1^{\mathrm{G}_1}} = k(\ln J)\mathbf{I} + 2\mu_{G_1}\prod_{1}^{\mathrm{G}_1} = \mathbf{C}_0^{\mathrm{G}_1}\colon \prod_{1}^{\mathrm{G}_1} \tag{25a}$$

$$\boldsymbol{\tau}_{G_2} = J\boldsymbol{\sigma}_{G_2} = \frac{\partial W}{\partial \prod_1^{\mathrm{G}_2}} = k(\ln J)\mathbf{I} + 2\mu_{G_2}\prod_{1}^{\mathrm{G}_2} = \mathbf{C}_0^{\mathrm{G}_2}\colon \prod_{1}^{\mathrm{G}_2} \tag{25b}$$

where $J = \lambda_1\lambda_2\lambda_3$ is the volume ratio of deformation, $\boldsymbol{\tau}_{G_1}$ and $\boldsymbol{\tau}_{G_2}$ represent Kirchhoff stress tensors of network A and B, $\boldsymbol{\sigma}_{G_1}$ and $\boldsymbol{\sigma}_{G_2}$ are the Cauchy stress tensors of network A and B, respectively. Besides, $\mathbf{C}_0$ is isotropic elasticity tensor and takes the form:

$$\mathbf{C}_0 = \mathrm{k}\mathbf{I} \otimes \mathbf{I} + 2\mu_G \mathrm{II} \tag{26}$$

with $\mathrm{II}_{ijkl} = \frac{1}{2}(\delta_{ik}\delta_{jl} + \delta_{il}\delta_{jk})$.

Utilizing the isochoric part of Hencky's strain energy function, the strain energy equation can be simplified as:

$$\mathrm{W}_{\mathrm{G}_1} = \mu_{\mathrm{G}_1}\left(\ln \mathbf{U}_{G_1}^{\mathrm{e}}\right)\colon \left(\ln \mathbf{U}_{G_1}^{\mathrm{e}}\right) \tag{27a}$$

$$\mathrm{W}_{\mathrm{G}_2} = \mu_{\mathrm{G}_2}\left(\ln \mathbf{U}_{G_2}^{\mathrm{e}}\right)\colon \left(\ln \mathbf{U}_{G_2}^{\mathrm{e}}\right) \tag{27b}$$

where elastic extension tensor can be determined by polar decomposition from elastic deformation gradient, which satisfies $\mathbf{F}_{G_1}^{e} = \mathbf{R}_{\mathrm{G}_1}^{\mathrm{e}}\mathbf{U}_{\mathrm{G}_1}^{\mathrm{e}}$ with $\mathbf{R}_{G_1}^{e}\mathbf{R}_{G_1}^{e\ T} = \mathbf{I}$ and $\mathbf{F}_{G_2}^{\mathrm{e}} = \mathbf{R}_{\mathrm{G}_2}^{\mathrm{e}}\mathbf{U}_{\mathrm{G}_2}^{\mathrm{e}}$ with $\mathbf{R}_{G_2}^{e}\mathbf{R}_{G_2}^{e\ T} = \mathbf{I}$. Consequently, the deviatoric part of the Cauchy stress tensor can be further given by:

$$\mathbf{T}_{\mathrm{G}_1} = \frac{2\mu_{\mathrm{G}_1}}{J}\mathbf{R}_{G_1}^{\mathrm{e}}\left(\ln \mathbf{U}_{G_1}^{e}\right)\mathbf{R}_{G_1}^{e\ T},\ \mathbf{T}_{\mathrm{G}_2} = \frac{2\mu_{\mathrm{G}_2}}{J}\mathbf{R}_{G_2}^{\mathrm{e}}\left(\ln \mathbf{U}_{G_2}^{e}\right)\mathbf{R}_{G_2}^{e\ T} \tag{28}$$

3.6.2. Viscous flow rule of the glassy phase

The contribution of network A to viscoelastic response increases monotonically with the increase of deformation. Furthermore, researches indicate that the relationship between stress and strain exhibits a certain power-law relation. Consequently, a power-law relation equation is introduced to describe the evolution law of nonlinear viscoelastic deformation:

$$M_{G_1} = \frac{3}{2}\eta_A D_{G_1} = P_{G_A}(exp\xi - 1)\left(\frac{D_{G_1}}{D_0}\right)^{n_A} \tag{29}$$

where η_A represents viscosity, P_{G_A} represents viscous parameter, ξ is scalar deformation, D_0 is reference strain rate, and n_A characterizes the rate sensitivity of network A.

The overall viscoelastic response of network B is similar to the

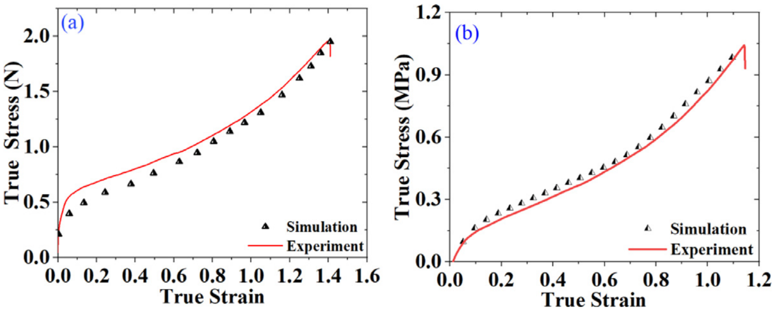

Fig. 11. Comparisons between simulated results and uniaxial tensile experiments at 90°C with loading rates of (a) 1000 mm/min (b) 1 mm/min.

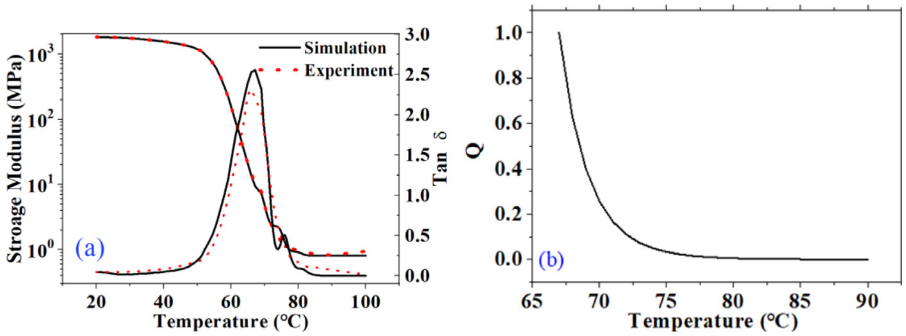

Fig. 12. Identification of the model parameters (a) Comparison between the predicted results and experimental results (b) Variation of parameter Q defined by Eq. (20) changes with temperature.

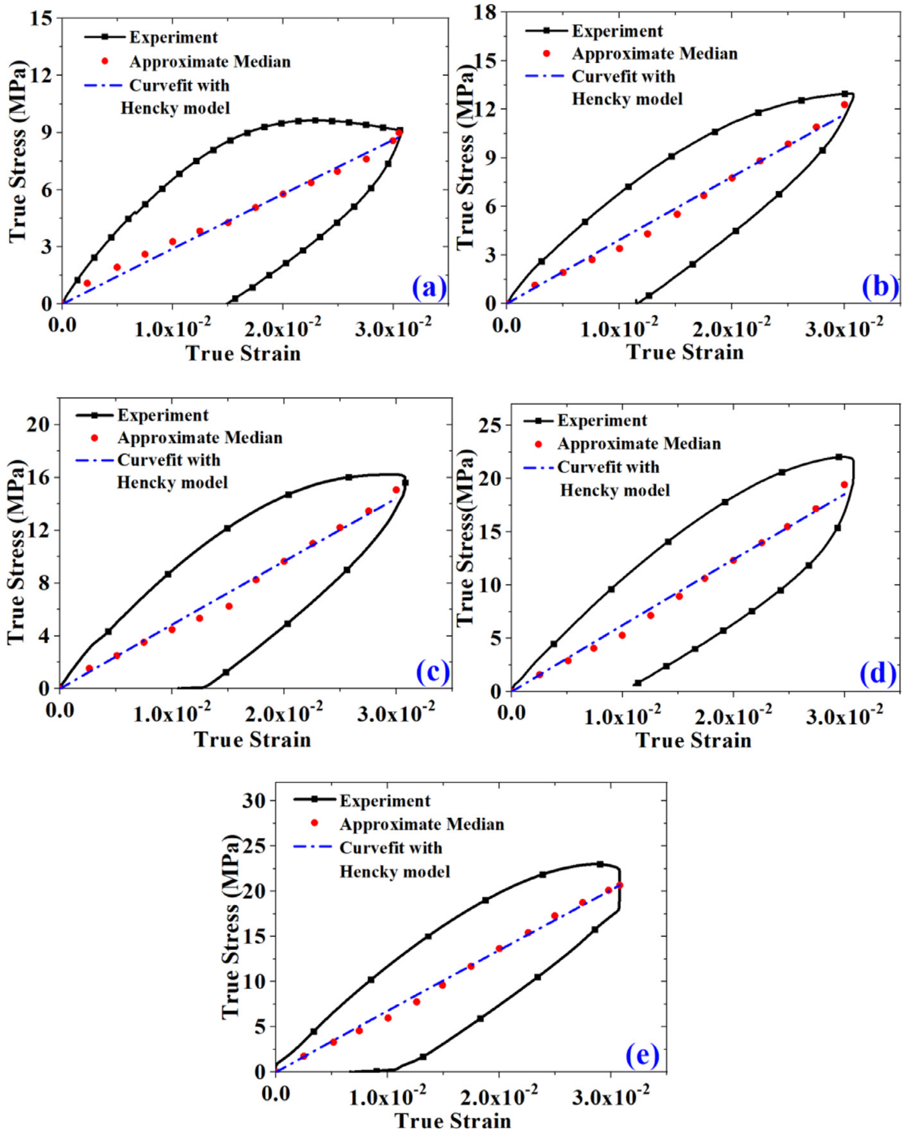

Fig. 13. Estimations of the viscous behavior of SMP at 35 °C with different loading rates (a) 1 mm/min (b) 5 mm/min (c) 10 mm/min (d) 20 mm/min (e) 50 mm/min.

Maxwell model composed of a spring (of Young's modulus E) and a dashpot (of viscosity η). The viscoelastic response of a Maxwell model can be expressed as (Brinson et al., 2008):

$$\sigma = E\tau\dot{\varepsilon}\left[1 - exp\left(-\frac{\varepsilon}{\tau\dot{\varepsilon}}\right)\right] \tag{30}$$

where $\tau = \frac{\eta}{E}$ is the relaxation time, and $\dot{\varepsilon}$ represents the strain rate. By introducing a rate sensitivity parameter, the equation can be further expressed as:

$$\sigma = \eta\dot{\varepsilon}\left[1 - exp\left(-\frac{\varepsilon}{\tau\dot{\varepsilon}}\right)^{n}\right] \tag{31}$$

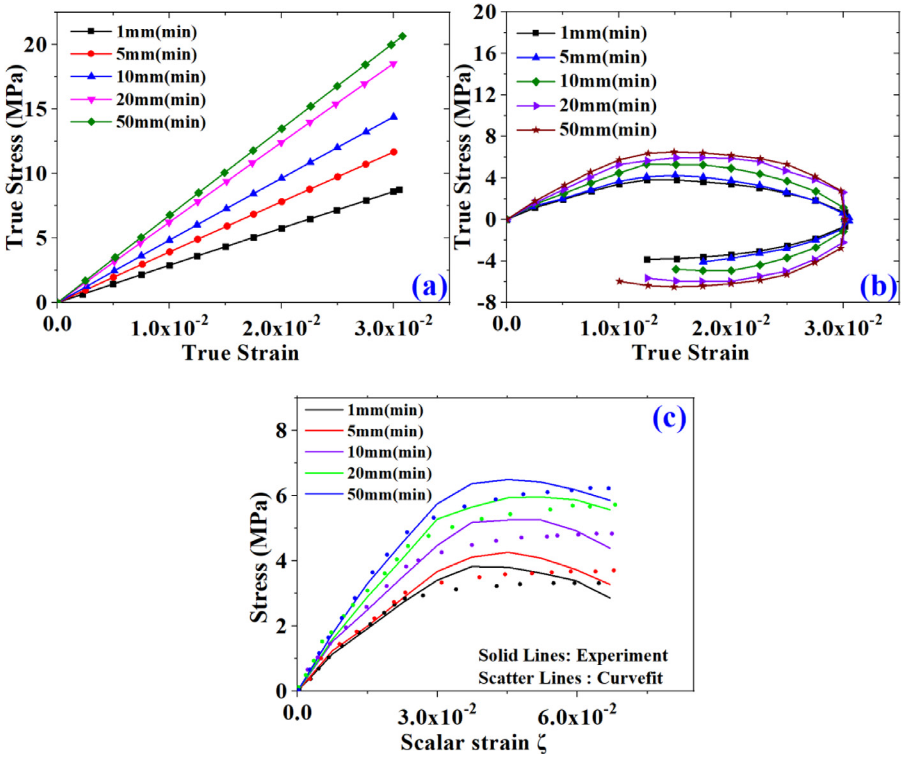

Fig. 14. Identification of the viscoelastic model parameters of glassy phase model (a) Estimations of the mechanical behavior of Network A using the modified equilibrium path concept (b) Estimations of the mechanical behavior of Network B using the modified equilibrium path concept (c) Equivalent Mandel stress changes with scalar deformation ζ.

Table 1
Summary of model parameters.

Parameter	Value	Physical meaning
α_G	1.29×10^{-4} /°C	CTE of glassy phase
α_R	3.06×10^{-4} /°C	CTE of rubbery phase
T_g	67 °C	Glass transition temperature
c_1	15.44	WLF parameter
c_2	75.62	WLF parameter
c_3^{R2}	1.8 MPa	Mooney-Rivlin model constant
c_4^{R2}	−1.1 MPa	Mooney–Rivlin model constant
c_3^{R1}	1.65 MPa	Mooney-Rivlin model constant
c_4^{R1}	−0.95 MPa	Mooney-Rivlin model constant
H_G	2.9	Model parameter
n_B	0.0966	Sensitivity control parameter
n_A	0.16	Sensitivity control parameter
μ_{G1}	316.28 MPa	Hencky model constant
μ_{G2}	242.13 MPa	Hencky model constant
η_R	9.562×10^3 Pa s^{-1}	Viscosity in the rubbery state
Q	2.5	Model parameter
p_{GA}	5.6 MPa	Viscous coefficient
p_{GB}	411.4 MPa	Viscous coefficient

with $\eta = -\frac{S}{\gamma_v}$.

Inspired by the one-dimensional Maxwell equation (Eq. (31)), the expression of three-dimensional deformation of network B is given by:

$$M_{G_2} = \mu_{G_2} H_G \left(\frac{D_{G_2}}{D_0}\right)\left\{1 - exp\left[-\frac{\zeta}{H_G}\left(\frac{D_{G_2}}{D_0}\right)^{-n_B}\right]\right\}, \zeta = \sqrt{tr\left(\mathbf{C}^e_{G_2}\right) - 3} \tag{32}$$

where ζ is scalar deformation, $\mathbf{C}^e_{G_2} = \mathbf{F}^T\mathbf{F}$ is the right Cauchy-Green tensor, and H_G represents viscous parameter of network B.

4. Identification of the model parameters

4.1. Constitutive equations for uniaxial loading condition

For uniaxial loading, the macroscopic stress tensor can be expressed as:

$$\boldsymbol{\sigma} = \sigma_1 \mathbf{e}_1 \otimes \mathbf{e}_1 \tag{33}$$

The macroscopic deformation gradient can be expressed as:

$$\mathbf{F}_{tot} = \lambda_1 \mathbf{e}_1 \otimes \mathbf{e}_1 + \lambda_2(\mathbf{e}_2 \otimes \mathbf{e}_2 + \mathbf{e}_3 \otimes \mathbf{e}_3) \tag{34}$$

with $J = det(F_{tot}) = \lambda_1\lambda_2^2$. The deviatoric part of the deformation gradient can be further expressed as a function of λ:

$$\mathbf{F} = \lambda \mathbf{e}_1 \otimes \mathbf{e}_1 + \frac{1}{\sqrt{\lambda}}(\mathbf{e}_2 \otimes \mathbf{e}_2 + \mathbf{e}_3 \otimes \mathbf{e}_3), \lambda = \left(\frac{\lambda_1}{\lambda_2}\right)^{\frac{2}{3}} \tag{35}$$

The general stretch deformation can be further divided into an elastic part ($\lambda^e_{G_1}, \lambda^e_{G_2}, \lambda^e_{R_1}$ and $\lambda^e_{R_2}$) and a viscous part ($\lambda^v_{G_1}, \lambda^v_{G_2}$ and $\lambda^v_{R_1}$):

$$\lambda = \lambda_G^M \lambda_G^T, \lambda = \lambda_R^M \lambda_R^T \tag{36-a}$$

$$\lambda_G^M = \lambda^e_{G_1}\lambda^v_{G_1} = \lambda^e_{G_2}\lambda^v_{G_2}, \lambda_R^M = \lambda^e_{R_1}\lambda^v_{R_1} = \lambda^e_{R_2} \tag{36-b}$$

On this basis, kinematic variables in the constitutive model can be expressed as the equation of elastic and viscous stretch, as well as the derivatives of time:

$$tr\mathbf{C}^e_{G_1} = \left(\lambda^e_{G_1}\right)^2 + \frac{2}{\lambda^e_{G_1}}, tr\mathbf{C}^e_{G_2} = \left(\lambda^e_{G_2}\right)^2 + \frac{2}{\lambda^e_{G_2}} \tag{37}$$

$$\ln \mathbf{U}^e_{G_1} = \ln \lambda^e_{G_1}\left(\mathbf{e}_1 \otimes \mathbf{e}_1 - \frac{1}{2}\mathbf{e}_2 \otimes \mathbf{e}_2 - \frac{1}{2}\mathbf{e}_3 \otimes \mathbf{e}_3\right) \tag{38a}$$

$$\ln \mathbf{U}^e_{G_2} = \ln \lambda^e_{G_2}\left(\mathbf{e}_1 \otimes \mathbf{e}_1 - \frac{1}{2}\mathbf{e}_2 \otimes \mathbf{e}_2 - \frac{1}{2}\mathbf{e}_3 \otimes \mathbf{e}_3\right) \tag{38b}$$

$$\zeta = \sqrt{\lambda^2 + \frac{2}{\lambda} - 3} \tag{39}$$

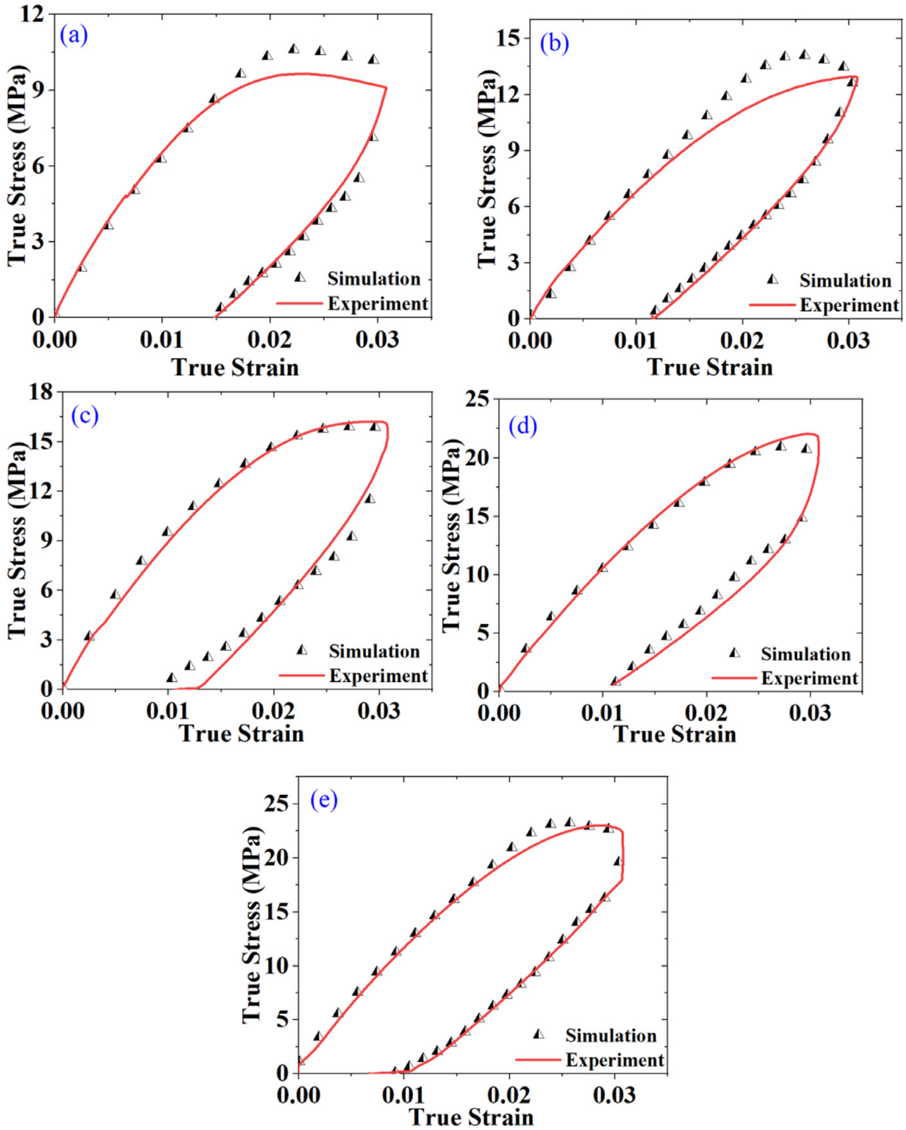

Fig. 15. Comparisons between simulations and experiments of loading-unloading cycles (a) 1 mm/min (b) 5 mm/min (c) 10 mm/min (d) 20 mm/min (e) 50 mm/min.

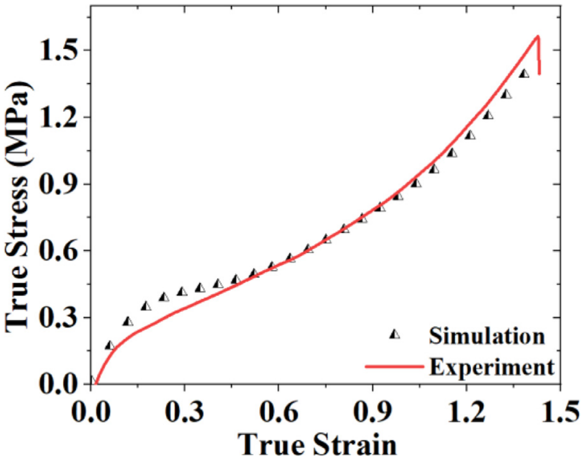

Fig. 16. Comparison between simulated and experimental results of the rubbery phase with a loading rate of 500 mm/min.

$$D_{G_1} = \frac{\dot{\lambda}_{G_1}^{v}}{\lambda_{G_1}^{v}},\; D_{G_2} = \frac{\dot{\lambda}_{G_2}^{v}}{\lambda_{G_2}^{v}} \tag{40}$$

Utilizing Eqs. (33)-(40) and the constitutive models of each network, the simplified constitutive relations under uniaxial loading can be obtained:

(1) The hydrostatic stress caused by volume deformation can be expressed as:

$$\sigma = \frac{k}{J}(\Theta_M - 1) \tag{41}$$

where $k = \frac{2\mu(1+\upsilon)}{3(1-2\upsilon)}$ is volume modulus and can be obtained by shear modulus $\mu = \Phi_G\mu_G + \Phi_R\mu_R$ and Poisson ratio υ.

(1) Mooney-Rivlin elasticity of rubbery network

For the two hyperelastic elements of the rubbery phase, the Cauchy stress under uniaxial loading can be calculated as:

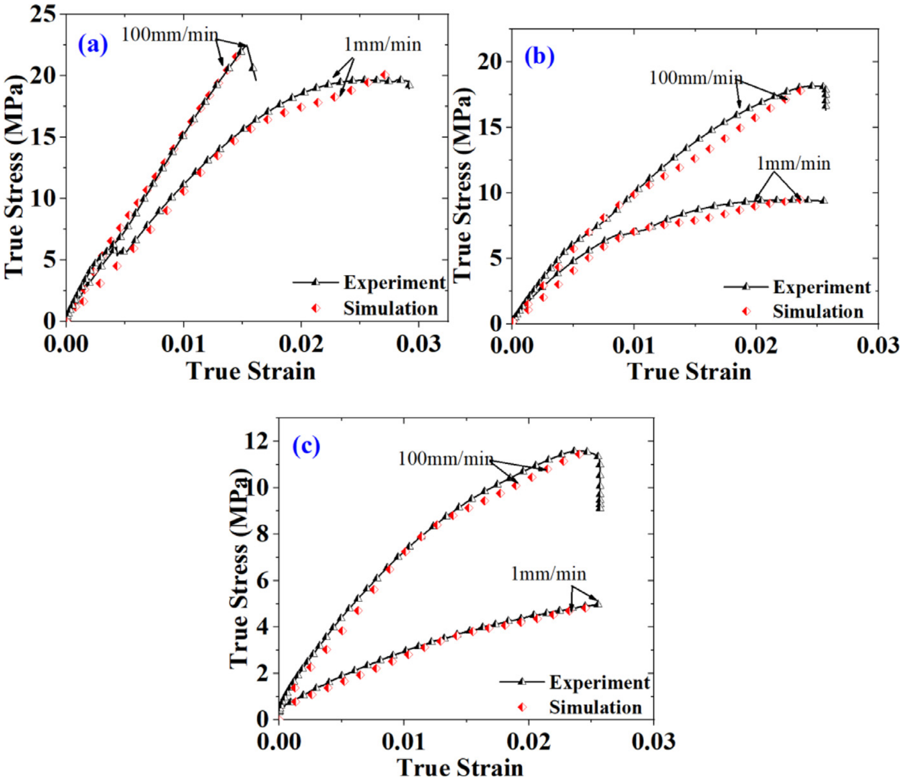

Fig. 17. Comparisons between simulated and experimental results with different temperatures and loading rates (a) Stress-strain curves at 25 °C (b) Stress-strain curves at 35 °C (c) Stress-strain curves at 45 °C.

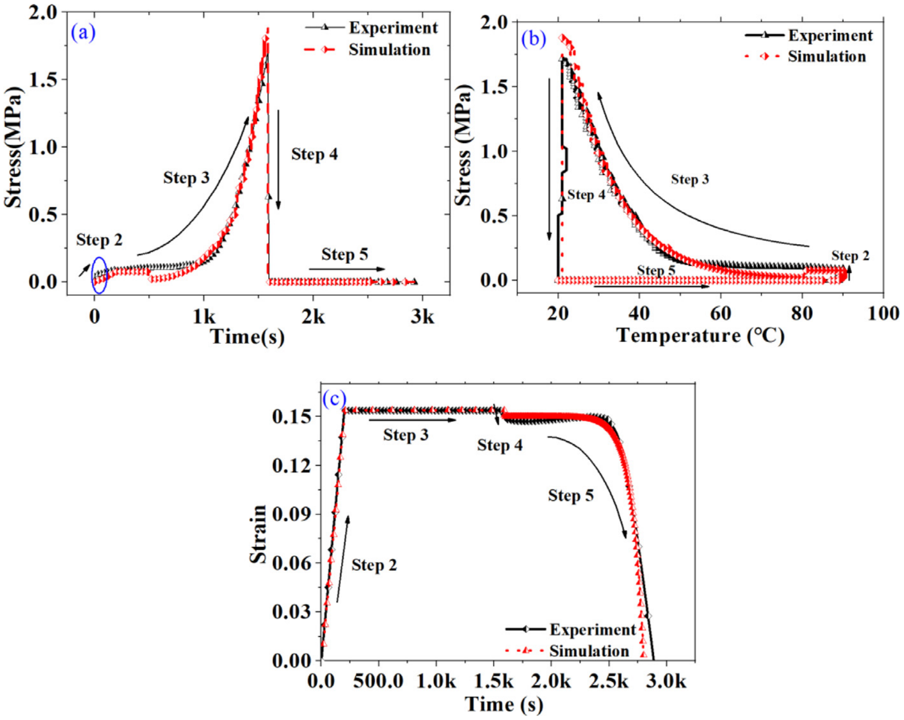

Fig. 18. Comparisons between simulated results and experiments of thermo-mechanical cycle experiments (a) stress history changes with time (b) stress history changes with temperature (c) strain history changes with time.

$$\sigma_R = \left(2c_3^{R_1} + \frac{2c_4^{R_1}}{\lambda_{R_1}}\right)\left(\lambda_{R_1}^2 - \frac{1}{\lambda_{R_1}}\right) \tag{42-a}$$

$$\sigma_R = \left(2c_3^{R_2} + \frac{2c_4^{R_2}}{\lambda_{R_2}}\right)\left(\lambda_{R_2}^2 - \frac{1}{\lambda_{R_2}}\right) \tag{42-b}$$

(1) Mechanical behavior of nonlinear viscous of the rubbery phase

For the viscous element in rubbery phase, the Cauchy stress can be expressed as:

$$\sigma_R = \eta_R \frac{\dot{\lambda}_R}{\lambda_R} \tag{43}$$

where λ_R and $\dot{\lambda}_R$ represents the stretch ratio and the time derivative of stretch ratio, respectively.

(1) Hencky elasticity in the glassy phase branch

For the two hyperelastic elements of the glassy phase, the constitutive relation of Cauchy stress can be calculated as:

$$\sigma_{G_1} = \frac{3\mu_{G_1}}{J} ln\lambda_{G_1} \tag{44a}$$

$$\sigma_{G_2} = \frac{3\mu_{G_2}}{J} ln\lambda_{G_2} \tag{44b}$$

(1) The nonlinear viscous response of network A

For the viscous element in network A, the Cauchy stress can be expressed as:

$$\sigma_{GA} = p_{G_A}(exp\zeta - 1)\left(\frac{D_{G_1}}{D_0}\right)^{n_A} \tag{45}$$

(1) The nonlinear viscous response of network B

For the viscous element in network B, the Cauchy stress can be expressed as:

$$\sigma_{GB} = p_{G_B} H_{GB}\left(\frac{D_G^v}{D_0}\right)^n \left\{1 - exp\left[-\frac{\varsigma}{\mathrm{H}_{G_B}}\left(\frac{D_G^v}{D_0}\right)^{-n_B}\right]\right\} \tag{46}$$

Set $\varsigma = \mathrm{H}_G(\frac{D_G^v}{D_0})^n$, then the equation can be simplified to:

$$\sigma_G = \mu_G \varsigma\left[1 - exp\left[-\frac{\varsigma}{\varsigma_G}\right]\right] \tag{47}$$

The total Cauchy stress of the model can be rewritten as:

$$\sigma = \Phi_G(\sigma_{G_1} + \sigma_{G_2}) + \Phi_R(\sigma_{R_1} + \sigma_{R_2}) + p\mathbf{I} \tag{48}$$

where σ is Cauchy stress, σ_R and σ_G are the stresses of the glassy phase and rubbery phase, respectively, and p represents hydrostatic stress. The overall strain-stress response can be calculated as:

$$\begin{aligned}\sigma \quad &= \Phi_G\left(\tfrac{3\mu_{G1}}{J} ln\lambda_{G_1} + \tfrac{3\mu_{G2}}{J} ln\lambda_{G_2}\right) + \Phi_R\left(2c_3 + \tfrac{2c_4}{\lambda}\right)\left(\lambda^2 - \tfrac{1}{\lambda}\right)\\ &+ \Phi_G k_G[J - 1 - 3\alpha_G(T - T_0)] + \Phi_R k_R[J - 1 - 3\alpha_R(T - T_0)]\end{aligned} \tag{49}$$

4.2. Determination of the model parameters of the phase transition process

According to the assumption of the "phase transition" concept, the transition process between the rubbery phase and the glassy phase will be continuous with the change of temperature, and the macroscopic display is shape memory effect. Based on the thermal-mechanical cycle test, the model parameters in Eq. (7) can be determined by the nonlinear fitting. The comparison between experiment and simulation is shown in Fig. 10, which reveals that Eq. (7) can approximately characterize the volume fraction of the glassy phase changing with temperature.

4.3. Determination of material parameters of the rubbery phase

According to the characteristics of viscoelastic materials, when the loading rate is large enough, the viscous response can be ignored. In order to obtain the model parameters of the rubbery phase, the experiment data with a loading rate of 1000 mm/min are adopted to fit the parameter. It is assumed that the effect of viscoelastic response can be neglected under this loading rate. For the rubbery phase model, due to $\mathbf{F}_\mathrm{R}^\mathrm{M} \cong \mathbf{F}_R^e$, the model parameters of $c_3^{R_2}$ and $c_4^{R_2}$ in the Mooney-Rivlin model can be determined from the best fitting of the stress-strain curve. The other model parameters $c_3^{R_1}$ and $c_4^{R_1}$ can be obtained by fitting the stress-strain curve with a loading rate of 1 mm/min. Meanwhile, by using the remaining experimental results with other loading rates, the deformation gradient $\mathbf{F}_\mathrm{R}^\mathrm{e}$ can be obtained. Based on the relationship $\mathbf{F}_\mathrm{R}^\mathrm{M} = \mathbf{F}_\mathrm{R}^\mathrm{e}\mathbf{F}_R^v$, the viscoelastic response of the rubbery phase can be further derived. From the fitting results, as shown in Fig. 11, it can be seen that this model can reproduce the experimentally observed results. On the basis, it can be obtained $c_3^{R_2} = 1.8$ MPa, $c_4^{R_2} = -1.1$ MPa, $c_3^{R_1} = 1.65$ MPa and $c_4^{R_1} = -0.95$ MPa.

The viscoelastic response of the rubbery phase can be captured by Eq. (20). The variation tendency of parameter Q changing with temperature can be obtained by the DMA curve (More details can be found in the Supporting Information, Appendix A). The comparison between simulation and experiment is shown in Fig. 12(a). Based on the simulation result, the corresponding parameters including c_1, c_2 and relaxation time can be determined. Subsequently, the model parameter Q changing with temperature can be further calculated as shown in Fig. 12(b). According to the phase transition hypothesis, when the temperature is higher than T_g, SMP shows a more obvious characteristic of the rubbery phase. Consequently, parameter Q can take an arbitrary value with a temperature higher than T_g. Here, it takes $Q = 2.5$ with a temperature of 90 °C.

4.4. Determination of material parameters of the glassy phase

According to the modified "equilibrium path" assumption, the contribution of elastic dominated deformation is presented by Network A while the contribution of viscous dominated deformation is represented by Network B. Consequently, the test curves can be divided into two parts bounded by the modified equilibrium path as shown in Fig. 13(a)–(e). It is not hard to see that stress under the same strain changes dramatically with the increase of loading rate. Exemplified by the limit loads under different loading rates, the maximum stress is 9.62 MPa with a loading rate of 1 mm/min and 22.96 MPa with a loading rate of 50 mm/min.

Combined with Eqs. (36), (44), (45) and (46), the contributions of elastic part and viscous part are shown in Fig. 14(a) and Fig. 14(b). Model parameters (μ_{G1}, μ_{G2}, H_G, n_A, n_B, p_{G_A}, p_{G_B}) for the glassy phase can be determined iteratively. As mentioned above, when the loading rate is high enough, it is considered that the viscoelastic response can be ignored, that is, $\lambda_{G_1}^M \cong \lambda_{G_1}^e$. Consequently, model parameters μ_{G_1} can be estimated by the stress-strain curve with the highest loading rate shown in Fig. 14(a). At the same time, utilizing the remaining stress-strain curves with other loading rates, the elastic deformation $\lambda_{G_1}^e$ can be calculated based on μ_{G_1}. Subsequently, utilizing the relationship $\lambda = \lambda_{G_1}^e\lambda_{G_1}^v$, the viscous coefficient can be determined. In the same way, utilizing the stress-strain curves in Fig. 14(b), the model parameters μ_{G_2}, $p_{G_B}$and n_B related to network B can be obtained. Furthermore, the corresponding equivalent Mandel stress versus scalar deformation ζ corresponding to each experiment can be calculated as shown in Fig. 14(c).

In this section, the related parameters of this model are determined and listed in Table 1.

5. Comparisons between simulated and experimental results

Based on the proposed model, the mechanical responses such as rate-dependent behavior, thermal-mechanical cycles and loading-unloading cycles are predicted. The comparisons between simulated results and experimental results indicate that the proposed model can reproduce the stress-strain response obtained by the experiments.

Fig. 15(a)–(e) illustrates the comparisons between simulations and experiments with different loading-unloading rates. By combining the stress of the elastic part represented by network A and the viscous part represented by network B, the overall stress-strain relation can be obtained. The comparisons indicate that the constitutive model can reproduce the experimental results and can capture the rate-dependent behaviors of SMP with different loading rates. Even though there are some differences in the maximum stress during the loading process, evolutionary trends are the same.

When the test temperature is 90 °C, SMP is entirely composed of the rubbery phase. The comparison between the predicted result and the experimental result of the rubbery phase is presented in Fig. 16. Based on the rubbery phase model of Network C and D, the predicted result indicates that it may capture the rate-dependent behavior and reproduce the experimental results.

The validity of the model was further verified by rate-dependent experiments with different temperatures and loading rates, as shown in Fig. 17(a)–(c). Loading rates were 1 mm/min and 100 mm/min with a test temperature of 25 °C, 35 °C and 45 °C, respectively. The comparisons indicated that the model could capture the variation trends and reproduce the viscoelastic behavior of SMP.

Furthermore, the predicted results of the thermal-mechanical cycle are compared with the experiment, as shown in Fig. 18. Based on the developed model, the simulation reproduces the thermal-mechanical cycle process of SMP. The results indicate that the variation history of stress changing with time (Fig. 18(a)) and temperature (Fig. 18(b)) can be well captured by the proposed model. When SMP is reheated above T_g, the strain recovery process will be activated. The simulation and experiment results are found to be mostly in agreement with the presented theories, whereby the new theory is feasible as shown in Fig. 18(c).

6. Conclusion

A constitutive model based on the multiplicative decomposition of the deformation gradient is established to describe the mechanical response of SMP based on the “phase transition” concept and rheological method. Mechanical behaviors of the glassy phase and rubbery phase are described by different constitutive structures. For the glassy phase, the “equilibrium path” concept is introduced and amended to describe the rate-dependent behavior of SMP. Furthermore, two Mooney-Rivlin models and a viscous element are introduced to describe the mechanical response of the rubbery phase. A series of mechanical tests including rate-dependent experiments, loading/unloading cycle tests and thermal-mechanical cycle tests are carried out to verify the validity of the proposed constitutive model. The comparisons show that a remarkable consistency exists between model predictions and experiments, and the current constitutive model can capture the non-linear viscoelastic deformation and the thermal-mechanical cycle of SMP.

Acknowledgments

This work was supported by the National Natural Science Foundation of China (Grant no. 11632005, 11672086) and by the Foundation for Innovative Research Groups of the National Science Foundation of China (Grant no. 11421091).

Supplementary materials

Supplementary material associated with this article can be found, in the online version, at doi:10.1016/j.mechmat.2019.103263.

References

Anand, L., 1979. On H. hencky's approximate strain-energy function for moderate deformations. J. Appl. Mech. 46, 78–82.
Bergström, J., Boyce, M., 1998. Constitutive modeling of the large strain time-dependent behavior of elastomers. J. Mech. Phys. Solids. 46, 931–954.
Brinson, H., Brinson, L., 2008. Polymer Engineering Science and Viscoelasticity: An Introduction. Springer Science + Business Media, LLC, New York, NY, pp. p.327.
Castano, L., Flatau, A., 2014. Smart fabric sensors and e-textile technologies: a review. Smart Mater. Struct. 23, 053001.
Chen, J., Liu, L., Liu, Y., Leng, J., 2014. Thermoviscoelastic shape memory behavior for epoxy-shape memory polymer. Smart Mater. Struct. 23, 055025.
Chen, Y., Lagoudas, D., 2008. A constitutive theory for shape memory polymers. Part I: large deformations. J. Mech. Phys. Solids. 56 (5), 1752–1765.
Diani, J., Gilormini, P., Fredy, C., Rousseau, I., 2012. Predicting thermal shape memory of crosslinked polymer networks from linear viscoelasticity. Int. J. Solids. Struct. 49 (5), 793–799.
Gu, J., Sun, H., Fang, C., 2015. A phenomenological constitutive model for shape memory polyurethanes. J. Intel. Mat. Syst. Str. 26 (5), 517–526.
Hencky, H., 1928. Über die Form des Elastizitätsgesetz bei ideal elastischen Stoffen. Z. Techn. Phys. 9, 215–220.
Holzapfel, G., 1999. Nonlinear Solid Mechanics: A Continuum Approach for Engineering. Wiley, New York, pp. 286–289.
Kim, J., Kang, T., Yu, W., 2010. Thermo-mechanical constitutive modeling of shape memory polyurethanes using a phenomenological approach. Int. J. Plasticity 26 (2), 204–218.
Kuenstler, A., Hayward, R., 2019. Light-induced shape morphing of thin films. Curr. Opin. Colloid. 40, 70–86.
Lendlein, A., Kelch, S., 2002. Shape Memory Polymers. Angewandte Chemie International Edition 41. pp. 2035–2057.
Liu, Z., Li, Q., Bian, W., Lan, X., Liu, Y., Leng, J., 2019. Preliminary test and analysis of an ultralight lenticular tube based on shape memory polymer composites. Compos. Struct. 223 (1), 110936.
Liu, Y., Gall, K., Dunn, M.L., Greenberg, A.R., Diani, J., 2006. Thermomechanics of shape memory polymers: uniaxial experiments and constitutive modeling. Int. J. Plasticity. 22, 279–313.
Liu, Y., Zhang, W., Zhang, F., Lan, X., Leng, J., Liu, S., Jia, X., Cotton, C., Sun, B., Gu, B., Chou, T., 2018. Shape memory behavior and recovery force of 4D printed laminated Miura-Origami structures subjected to compressive loading. Compos. Part B-Eng. 153, 233–242.
Lu, H., Wang, X., Xing, Z., Fu, Y., 2019. A cooperative domain model for multiple phase transition and complex conformational relaxations in polymers with shape memory effect. J. Phys. D-Appl. Phys. 52 (24), 245301.
Lv, H., Leng, J., Du, S., 2013. A phenomenological approach for the chemo-responsive shape memory effect in amorphous polymers. Soft Matter 9 (14), 3851–3858.
Mao, Y., Chen, F., Hou, S., Qi, J., Yu, K., 2019. A viscoelastic model for hydrothermally activated malleable covalent network polymer and its application in shape memory analysis. J. Mech. Phys. Solids. 127, 239–265.
Meiorin, C., Actis, D., Montoro, F., Londoño, O., Aranguren, M., Muraca, D., Zélis, P., Knobel, M., Mosiewicki, M., 2018. Magnetic remote activation of shape recovery in nanocomposites based on tung oil and styrene. Phys. Status. Solidi. A. 215 (24), 1800311.
Nguyen, T., Qi, H., Castro, F., Long, K., 2008. A thermoviscoelastic model for amorphous shape memory polymers: incorporating structural and stress relaxation. J. Mech. Phys. Solids. 56 (9), 2792–2814.
Park, H., Harrison, P., Guo, Z., Lee, M., Yu, W., 2016. Three-dimensional constitutive model for shape memory polymers using multiplicative decomposition of the deformation gradient and shape memory strains. Mech. Mater. 93, 43–62.
Qi, H., Nguyen, T., Castroa, F., Yakacki, C., ShandaSa, R., 2008. Finite deformation thermo-mechanical behavior of thermally induced shape memory polymers. J. Mech. Phys. Solids. 56 (5), 1730–1751.
Qi, H., Boyce, M., 2005. Stress-strain behavior of thermoplastic polyurethanes. Mech. Mater. 37, 817–839.
Tobushi, H., Okumura, K., Hayashi, S., Ito, N., 2001. Thermomechanical constitutive model of shape memory polymer. Mech. Mater. 33 (10), 545–554.
Urbina, L., Alonso-Varona, A., Saralegi, A., Palomares, T., Eceiza, A., Corcuera, M., Retegi, A., 2019. Hybrid and biocompatible cellulose/polyurethane nanocomposites with water-activated shape memory properties. Carbohyd. Polym. 216 (15), 86–96.
Westbrook, K., Kao, P., Castro, F., Ding, Y., Qi, J., 2011. A 3D finite deformation constitutive model for amorphous shape memory polymers: a multi-branch modeling approach for nonequilibrium relaxation processes. Mech. Mater. 43, 853–869.
Williams, M., Landel, R., Ferry, J., 1955. The temperature dependence of relaxation mechanisms in amorphous polymers and other glass-forming liquids. J. Am. Chem. Soc. 77, 3701–3707.
Xie, F., Huang, L., Liu, Y., Leng, J., 2014. Synthesis and characterization of high temperature cyanate-based shape memory polymers with functional polybutadiene/acrylonitrile. Polymer (Guildf) 55, 5873–5879.
Yin, C., Zeng, H., Gu, J., Xie, Z., Sun, H., 2019. Modeling the thermomechanical behaviors of particle reinforced shape memory polymer composites. Appl. Phys. A-Mater. 125

(6), 382.

Zhang, D., Liu, Y., Yu, K., Leng, J., 2011. Influence of cross-linking agent on thermomechanical properties and shape memory effect of styrene shape memory polymer. J. Intel. Mat. Syst. Str. 22 (18), 2147–2154.

Zhao, W., Liu, L., Zhang, F., Liu, Y., Leng, J., 2019. Shape memory polymers and their composites in biomedical applications. Mat. Sci. Eng. C-Mater. 97, 864–883.

Zhao, W., Wang, Q., Liu, L., Liu, Y., Leng, J., 2018. Structural response measurement of shape memory polymer components using digital image correlation method. Opt. Laser. Eng. 110, 323–340.

Zhao, W., Liu, L., Lan, X., Liu, Y., Leng, J., 2017. Adaptive repair device concept with shape memory polymer. Smart. Mater. Struct. 26, 025027.